SCIENTIFIC REPORTS

OPEN

SUBJECT AREAS:
POROUS MATERIALS
STRUCTURAL PROPERTIES
METAL-ORGANIC FRAMEWORKS
ORGANIC-INORGANIC NANOSTRUCTURES

Received
7 June 2013

Accepted
20 August 2013

Published
10 September 2013

Correspondence and requests for materials should be addressed to Z.S. (zmsu@nenu.edu.cn) or Y.L. (yqlan@njnu.edu.cn)

An unprecedented (3,4,24)-connected heteropolyoxozincate organic framework as heterogeneous crystalline Lewis acid catalyst for biodiesel production

Dong-Ying Du[1], Jun-Sheng Qin[1,2], Zhong Sun[1], Li-Kai Yan[1], Michael O'Keeffe[4], Zhong-Min Su[1,2], Shun-Li Li[3], Xiao-Hong Wang[1], Xin-Long Wang[1] & Ya-Qian Lan[3]

[1]Institute of Functional Material Chemistry, Faculty of Chemistry, Northeast Normal University, Changchun 130024, P. R. China, [2]State Key Laboratory of Supramolecular Structure and Materials, Jilin University, Changchun 130012, P. R. China, [3]Jiangsu Key Laboratory of Biofunctional Materials, College of Chemistry and Materials Science, Nanjing Normal University, Nanjing 210023, P. R. China, [4]Department of Chemistry and Biochemistry, Arizona State University, Tempe, Arizona 85287, United States.

A novel 3D hexadecanuclear heteropolyoxozincate organic framework, IFMC-200, has been successfully synthesized based on a late transition metal-oxygen cluster. IFMC-200 not only represents the first example of (3,4,24)-connected framework but also contains the first 24-connected single metal cluster in a crystal structure. It exhibits superior thermal stability, good water-stability, and even insensitivity to the existence of acid and base within a certain range of pH values. Furthermore, it performs as a heterogeneous crystalline Lewis acid catalyst with good activity for the conversion of long-chain fatty acids rather than short-chain ones, and high recycling efficiency for esterification reaction of fatty acids with alcohols to produce biodiesel.

Polyoxometalates (POMs), soluble anionic metal oxide clusters, are comprised of early-transition metal with d^0 or d^1 electronic configurations (usually $Mo^{VI/V}$, W^{VI}, V^V, Nb^V or Ta^V), which have attracted intense attention during the last two decades not only for their remarkable structural and electronic properties, but also for their intriguing applications ranging from catalysis to medicine[1–8]. The metal oxide clusters entirely consisted of late transition metal ions with d^{10} electronic configuration are rarely available owing to the instability of extremely high negative charge, though a series of addenda atoms substituted by late transition metal ions (such as Fe^{III}, Co^{II}, Cu^{II}, Mn^{II} and Zn^{II}) were commonly reported[9–11]. Compared with conventional POM clusters, d^{10} metal-oxygen clusters may have some special properties resulting from the inherent characteristics of late transition metals. In this regard, how to lower the overall negative charge to obtain d^{10} metal-oxygen clusters is a significant and challenging task in synthetic chemistry and material sicence[12,13].

Biodiesel, a renewable source of energy, seems to be an attractive candidate for the solution of global energy demands due to its environmental and sustainable benefits[14,15]. However, biodiesel is currently not competitive with the conventional diesel fuel because of its high costs of raw material and production processing[16–18]. That is, the presence of free fatty acids (FFAs) and water in low quality feedstocks would result in two undesirable side reactions, saponification and triglyceride hydrolysis, making the production process complicated. One way to overcome this problem is to subject FFAs to esterification before the transesterification of triglycerides. Thus, esterification is an essential step in the production of biodiesel and the search for highly efficient catalysts becomes greatly desirable in esterification reaction. In this context, heterogeneous catalysts, which are insoluble, easily separated from products, and reusable, exhibit important advantages with respect to homogeneous catalysts and become particularly important[19–22]. POM-based materials with Lewis and Brønsted acidity and reversible redox activity have been utilized as efficient solid acid and electron transfer catalysts for the production of industrially important chemicals since the late 1970s[23–28]. Recently, POM-based materials were also used as acid catalysts for biodiesel production[29–32]. In most cases, Lewis acidic POM-based catalysts could be obtained through the

following strategies: (i) exchanging protons with Lewis acidic cations, including Zn^{II}, Al^{III}, Sn^{IV}, Fe^{III} and so on[32], (ii) incorporation of rare earth metal ions into the vacant sites of POM ions[33,34], and (iii) supporting POMs on Lewis acidic porous materials, for instance, Ta_2O_5 and zeolites[31,35,36]. However, the above materials often encounter disadvantages, such as being homogeneous forms, difficulty in controlling synthesis, leaching of active sites from supports, hindering substrate accessing to catalytically active sites, and inferior activities compared to homogeneous analogues. Meanwhile, crystalline catalysts have caught increasing attention of researchers worldwide due to their well-defined crystalline structures, regular and tunable cavities and high catalytically active site density[37–39]. If organic ligands can directly bond to metal-oxygen clusters to achieve metal-oxygen clusters-based crystalline catalysts that meet the above-mentioned requirements, it may be a 'one stone two birds' method. So far, this kind of catalyst has not been reported for biodiesel preparation. Therefore, the search for design synthesis and development of environmentally benign catalysts which are highly active in water, higher thermodynamic stable, highly accessible to acid sites and recyclable is one of the most challenging issues in the production of biodiesel.

These inspired us to employ a semirigid ligand containing eight carboxyl groups, 5,5′-(2,2-bis((3,5-dicarboxyphenoxy)methyl)propane-1,3-diyl)bis(oxy) diisophthalic acid (H_8L, Figure S1)[40], and H_3PO_3 for the isolation of crystalline catalysts containing d^{10} metal-oxygen clusters, which gives the following considerations: (i) It is difficult to isolate classical metal-oxygen clusters from late transition metal ions due to the instability of extremely high negative charge. The substitution of terminal −O and μ_2−O of POM clusters with rich carboxyl groups of H_8L ligand would greatly reduce negative charge, which is beneficial to the formation of late transition metal-oxygen clusters. (ii) It is difficult to directly bond organic linkers to the traditional POM clusters owing to their oxygen-rich surface, so we intend to take the advantage of late transition metal ions to replace early ones to synthesize metal oxide cluster-organic frameworks. (iii) The introduction of H_3PO_3 is favorable to induce the formation of metal-oxygen clusters, which perhaps plays the role of heteroatom in the formation of hetero-POM anions. Fortunately, a novel heteropolyoxozincate containing hexadecanuclear zinc nanocluster, $[Zn_{16}(HPO_3)_4]L_3$ (**IFMC-200**, IFMC = Institute of Functional Material Chemistry), was successfully synthesized and structurally characterized. **IFMC-200** is stable in air and common organic solvents, and remarkably insensitive to the presence of water, even in acidic and basic aqueous solution within a certain range of pH values. Furthermore, **IFMC-200** was employed as a heterogeneous catalyst for the preparation of biodiesel, which is the first time to employ a crystalline material of entire d^{10} metal oxide cluster with Lewis acid nature.

Results

Single-crystal X-ray analysis. **IFMC-200** crystallizes in the cubic space group *F*-43*c* (219, Table S1) and consists of two kinds of Zn^{II} cations (Figure S2), HPO_3^{2-} anion and deprotonated L^{8-} ion. Each Zn(1) ion is tetrahedrally coordinated by three carboxylic oxygen atoms derived from three bridging L^{8-} fragments and one oxygen atom originated from HPO_3^{2-} ion. And each Zn(2) atom shows a octahedral geometry, which is completed by six oxygen atoms originated from three bridging L^{8-} ions and three HPO_3^{2-} ions. The P element in HPO_3^{2-} ion is in +3 oxidation state, and exhibits a tetrahedral configuration with the lone pairs pointing into the tetrahedral cavity, which has been observed in arsenolite (As_2O_3)[41]. In addition, twelve Zn(1) and four Zn(2) cations were connected by four HPO_3^{2-} anions, resulting in a nanocluster subunit $[Zn_{16}(HPO_3)_4]^{24+}$ (noted as $\{P_4Zn_{16}\}$, Figure 1a, left). To a certain extent, it is similar to classical Keggin-type cluser[42], which is composed of four internally edge sharing triads (M_3O_{13}) that share corners with each other and are disposed tetrahedrally around a central heteroatom with T_d symmetry (Figure 1a, right). As a result of the expansion of space among four HPO_3^{2-} ions, the size of $\{P_4Zn_{16}\}$ cluster in **IFMC-200** (with a diameter of ~13 Å) is clearly larger than that of Keggin-type anion (~10 Å). For conventional fully oxidized POM anions, especially Keggin ions, the highest occupied molecular orbital (HOMO) is mostly from 2p orbitals of the bridging-O atoms, whereas the lowest unoccupied molecular orbital (LUMO) is from 4d orbitals of Mo or W atoms[43]. However, the frontier molecular orbitals of **IFMC-200** show significant differences with those of traditional POM clusters owing to d^{10} electronic configuration of Zn^{II} cations. In **IFMC-200**, the carboxyl-O atoms that coordinate to Zn(2) atoms contribute to the HOMO, and the LUMO is mainly from p orbitals of carboxyl-C atoms (Figure S3). An interesting structural feature of **IFMC-200** is that each $\{P_4Zn_{16}\}$ cluster is stabilized by 24 carboxyl groups from twelve L^{8-} moieties and the connection of eight $\{P_4Zn_{16}\}$ clusters and six L^{8-} fragments generates one nanocage with dimensions of 11 × 11 × 11 Å (Figure 1b,c and S4). Such connectivity leads to a 3D open architecture (Figure 1d). PLATON calculations reveal that a free volume in **IFMC-200** is about 7786.2 $Å^3$ per unit cell (27.1% of the cell volume)[44].

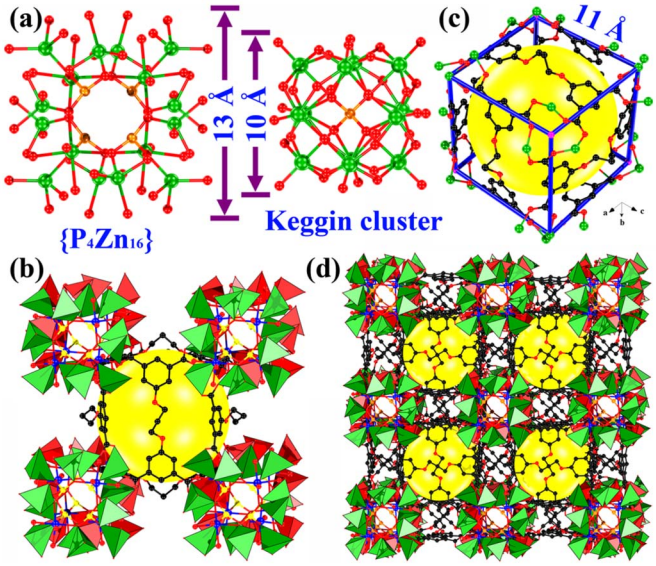

Figure 1 | (a) The structures of $\{P_4Zn_{16}\}$ (left) and Keggin-type cluster (right); (b) and (c) the cage structure in **IFMC-200**; and (d) the 3D framework of **IFMC-200**.

On the basis of topological analysis, the structure of **IFMC-200** can be considered as a 3D (3,4,24)-connected framework, if the center of the L^{8-} ligand is regarded as a 4-connected node, the $C_6H_3(COO)_2$ moiety as a 3-connected node, and the $\{P_4Zn_{16}\}$ cluster as a 24-connected node with a distorted rhombicuboctahedral geometry (Figure 2). The underlying trinodal net, which has been assigned the reticular chemistry structural resource (RCSR) symbol[45], **ddy**, was analyzed with the program Systre[46] which shows that it has intrinsic symmetry *Pm*-3*m* and is one of a special group of nets with the minimum number of kinds of edge (link) – in this case two for a trindal net. A maximum symmetry embedding is presented as a systre file in the Supplementary Information. It is worthy of note that the 24-connected node is essentially different from that documented in the literatures[47]. The previously-reported 24-connected node is really a tertiary building unit, constructed from twelve "paddle-wheel" dimetal tetracarboxylate secondary building units and may be further extended by functionalization at 5-position of 1,3-benzenedicarboxylate ligand (Figure S5)[48–50]. It should be pointed out that $\{P_4Zn_{16}\}$ cluster is the first real 24-connected node, which is an important discovery in topological crystal chemistry. From the data

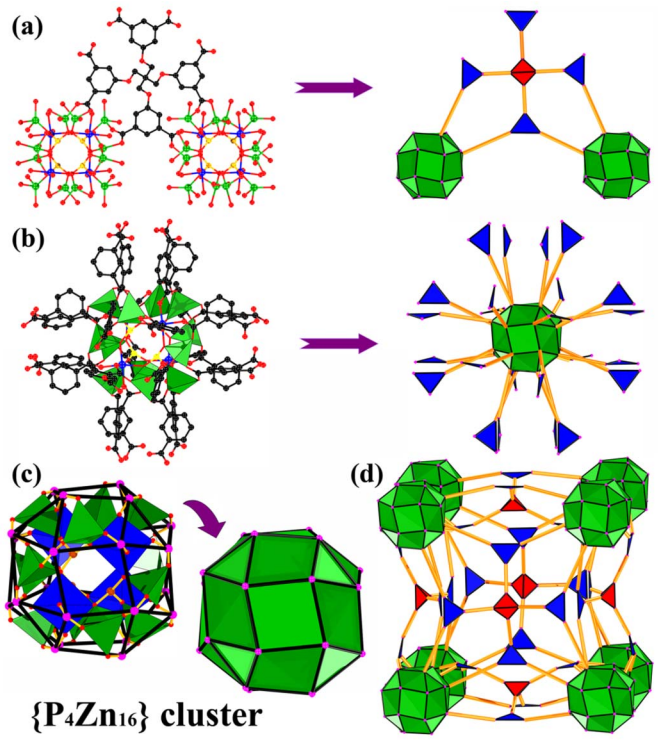

Figure 2 | The (3,4,24)-connected structure of IFMC-200. (a) the center of H_8L ligand as a 4-connected node, the $C_6H_3(COO)_2$ moiety as a 3-connected node; (b) and (c) the $\{P_4Zn_{16}\}$ cluster as a 24-connected node; and (d) the (3,4,24)-connected **ddy** topology.

in the RCSR, we found that **IFMC-200** is the first example of (3,4,24)-connected topology and the first undoubted 24-connected node constructed from a single cluster. Moreover, it was also not hypothesized in Euclidean Patterns in Non-Euclidean Tilings (EPINET)[51]. Offering further insight into this intricate architecture, the overall structure of **IFMC-200** can also be considered as a (4,12)-connected **ftw** topology framework when L^{8-} fragments are considered as 4-connected nodes and each $\{P_4Zn_{16}\}$ cluster corresponds to a 12-connected vertex (Figure S6)[52]. So far, only three topologies combine 4,12-connected components in the RCSR database, that is, **ith**, **shp**, and **ftw**. Notably, our group has reported a (4,12)-connected **ith** topology network (Figure S7)[53].

Discussion

Crystals of **IFMC-200** were isolated by hydrothermal reaction of $ZnCl_2$, H_3PO_3, $Na_2MoO_4{\cdot}2H_2O$, Mo powder, H_8L, and TBAOH (Tetrabutylammonium hydroxide). The parallel experiments suggest that **IFMC-200** cannot be obtained if there is no addition of $Na_2MoO_4{\cdot}2H_2O$ and Mo powder. Meanwhile, H_3PO_3 not only plays the role of phosphorus source but also structure-directing agent in the formation of $\{P_4Zn_{16}\}$ cluster because there is no product if H_3PO_3 was replaced with H_3PO_4. It is clear to see that **IFMC-200** formed a cubic shape under both optical microscopy and scanning electron microscopy (Figure S8). The corresponding EDS analysis reveals that there is no Mo element in **IFMC-200** although sodium molybdate dihydrate and Mo powder were introduced to the reaction system (Figure S9), which is in agreement with the result of single crystal X-ray diffraction. Phase purity of the bulky crystals was confirmed by the similarity between the experimental and simulated X-ray powder diffraction (XRPD) patterns (Figure S10). **IFMC-200** was generated in aqueous media; theoretically, it is stable in water even at different temperatures, as confirmed by subsequent XRPD and FT/IR measurements (Figure S10 and S11). It was also found that **IFMC-200** is stable in acidic and basic aqueous solution in the pH range of 2–12 (Figure 3 and S12). The vapour adsorption experiments for **IFMC-200** suggest that water is hardly adsorbed, but certain amounts of ethanol and cyclohexane are adsorbed (Figure S13). Thus, **IFMC-200** possesses hydrophobic cages. Furthermore, the thermogravimetric analysis (TGA) suggests that **IFMC-200** has exceptional thermal stability with decomposition starting at 450°C (Figure S14), which is much higher than that of Nafion NR50 (280°C), one of the most stable resins[54].

Generally, biodiesel can be prepared by transesterification of triglycerides or esterification of fatty acids with alcohols[55,56]. In terms of both atomic economy and green synthesis, heterogeneous solid state acid catalysts that work actively with easily separation for recyclability are highly desirable. The acid value of 0.61 $mmol{\cdot}g^{-1}$ for **IFMC-200** was detected by titration with aqueous ammonia, which is smaller than those of $ZnCl_2$ (7.96 $mmol{\cdot}g^{-1}$) and Keggin structure $Zn_{1.2}H_{0.6}PW_{12}O_{40}$ (1.14 $mmol{\cdot}g^{-1}$)[30], but higher than those of other Lewis solid state acid catalysts (e.g., Y-zeolites, 0.54 mmol $H^{+}{\cdot}g^{-1}$)[57]. In this regard, **IFMC-200** was evaluated as a heterogeneous catalyst in the esterification of fatty acids with a series of alcohols (Figure 4). The reactions were performed in the presence of an excess amount of alcohols with oil/alcohol molar ratio of 1 : 10 at 65°C. Preliminary studies were carried out to optimize the reaction conditions, and the results are presented in Figure S15, Table S2 and S3. The esterification reaction of palmitic acid with ethanol catalyzed by **IFMC-200** reached its highest conversion (44.7%) and turnover frequency (TOF, 26.4 h^{-1}) with catalyst amount of 1% wt total reactant weight in 10 h. In comparison, a blank experiment was also performed under the given conditions. The conversion of **IFMC-200** catalyzed esterification of palmitic acid with ethanol was 10 times higher than that in the case of no catalyst (4.3%). Furthermore, we used the conventional Lewis acid $ZnCl_2$ with higher acid value than **IFMC-200** as catalyst under the identical conditions, and the result suggested that **IFMC-200** showed higher TOF than $ZnCl_2$ (8.6 h^{-1}). This may be attributed to the poor water-tolerance of $ZnCl_2$. It is known that $ZnCl_2$ requires strictly anhydrous conditions because it immediately reacts with water forming in esterification of acids with alcohols, resulting in its serious decomposition[58]. **IFMC-200** is much more stable than $ZnCl_2$ in esterification reaction and could not be decomposed by water. With the optimal reaction time and catalyst amount, a series of fatty acids and alcohols were then examined under this condition and the results are collected in Table 1 and Figure S16. As can be seen from Table 1, the biodiesel conversion increased as the chain length of free fatty acids was increased, maintaining other constants. This result is opposite to the previous report[59], in which Goodwin et al. illustrated that the porous silica support would diminish the likelihood of mass diffusion limitation, making it favorable for the esterification reaction of low-molecular weight carboxylic acids. This abnormal result perhaps can be attributed to the positive effects of inorganic-organic hybrid framework of **IFMC-200** and the presence of hydrophobic cage structure in **IFMC-200**. It is well-known that the acidic catalysis depends on the acidic strength, as well as the concentration of substrates around the catalytic sites. **IFMC-200** located its Lewis acidic sites on the backbone of framework, and hydrophobic surroundings inside the pores. This unique structure feature provides long chain fatty acid molecules more chance to access to the catalytic sites due to their large lipophilicity. In other words, the long chain fatty acid molecules could be concentrated around the catalytic sites compared to short-chain ones. In addition, the hydrophobic cages could promote the water generating during the reaction to leach from the catalytic sites, which avoids the deactivation of the acid sites by water. Up to now, there are only few reports on solid porous catalysts with hydrophobic cages, just Inumaru's group firstly demonstrated $H_3PW_{12}O_{40}$ immobilized in hydrophobic nanospaces of organomodified mesoporous silica to show water-tolerant properties[60]. Therefore, **IFMC-200** exhibited

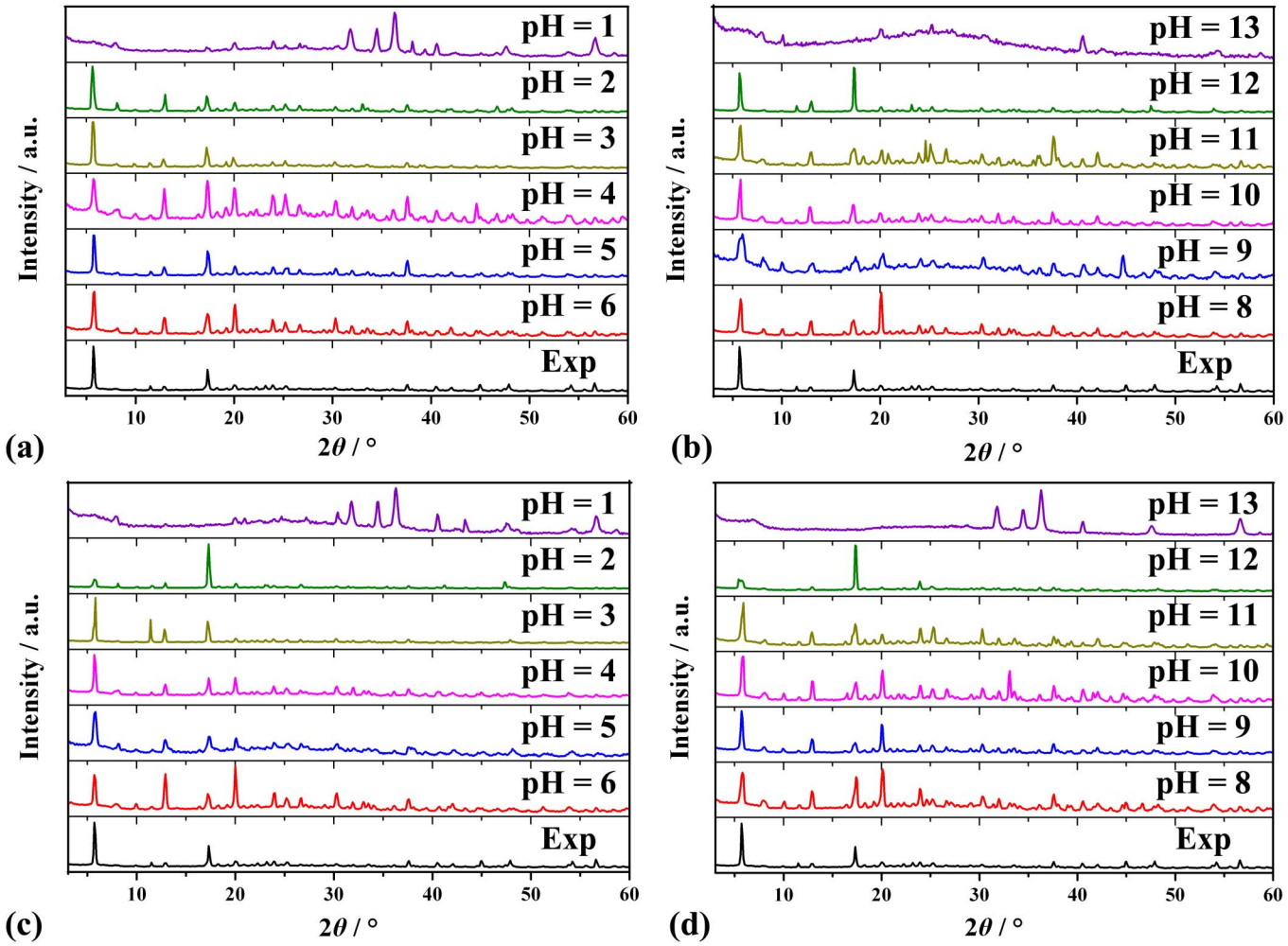

Figure 3 | The XRPD patterns of IFMC-200 after heated in Teflonlined stainless steel container at 65°C (a, b) and 140°C (c, d) for 12 h at different pH values, respectively. Exp represents XRPD pattern of **IFMC-200** without further treatment.

water-tolerant properties compared to conventional Lewis acid, $ZnCl_2$, generated by the existence of hydrophobic cages, which makes it favorable for esterification of long-chain carboxylic acids rather than short-chain ones. It might be the only one report on this opposite result. More importantly, **IFMC-200** showed very good recyclability. For example, there was almost no activity loss over **IFMC-200** after six times (Figure S17). This perhaps associated with the stable structure of **IFMC-200** (Figure S18 and S19). The excellent stability and recyclability of **IFMC-200** is potentially important for industrial applications.

Table 1 | The Con. (%) and TOF (h^{-1}) of **IFMC-200** catalyzed esterification of FFAs with alcohols. Conditions: 1% wt catalyst; 65°C; oil/alcohol molar ratio = 1 : 10; 10 h

Entry	Alcohols	Fatty acids	Con./%	TOF/h^{-1}
1	methanol	octanoic acid	8.8	5.3
2	methanol	lauric acid	20.4	12.3
3	methanol	palmitic acid	23.6	13.9
4	methanol	stearic acid	33.9	20.2
5	ethanol	octanoic acid	31.8	19.2
6	ethanol	lauric acid	46.1	25.6
7	ethanol	palmitic acid	44.7	26.4
8	ethanol	stearic acid	47.0	28.0
9	n-butanol	octanoic acid	62.8	37.9
10	2-methyl propanol	octanoic acid	62.2	37.6
11[a]	ethanol	palmitic acid	40.5	8.6
12[b]	ethanol	palmitic acid	4.3	_

[a]$ZnCl_2$ was used as catalyst.
[b]No catalyst was used.

In summary, we synthesized an unprecedented 3D (3,4,24)-connected heteropolyoxozincate organic compound, **IFMC-200**, which contains the first example of 24-connected node constructed from a single metal cluster. We have developed a new strategy with "carboxyl group-stabilized polyoxozincate cluster" mode that helps to lower the overall negative charge, and successfully proved that it is an efficient method to isolate late transition metal-oxygen cluster. **IFMC-200** exhibits superior thermal stability, good water-stability, tolerance to acid and base, and Lewis acidity, which enable its cata-

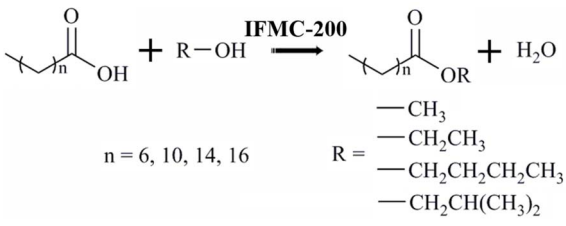

Figure 4 | The equation of IFMC-200 catalyzed esterification of FFAs with alcohols.

lytic activity in the esterification of carboxylic acids with alcohols. Surprisingly, **IFMC-200** exhibits abnormal catalytic result that is favor for the conversion of long-chain fatty acids under the same conditions compared to the previous reports. Further studies concerning this strategy for the synthesis of more late transition oxide cluster-based heterogeneous crystalline catalysts and their catalytic activities in the production of biodiesel are currently in progress.

Methods

Sample synthesis. 6 mL of distilled water was added to a beaker, which contains $Na_2MoO_4{\cdot}2H_2O$ (0.63 g, 2.6 mmol), Mo powder (0.05 g, 0.52 mmol), $ZnCl_2$ (0.14 g, 1.0 mmol), 50% H_3PO_3 (0.10 mL), and TBAOH with stirring for 15 min. Next, the pH value of the mixture was adjusted to 4.8 with 2 $mol{\cdot}L^{-1}$ HCl and then the mixture was stirred for another 15 min followed by the addition of H_8L (0.12 g, 0.15 mmol). Then the mixture was transferred and sealed in a 23 mL Teflonlined stainless steel container, and cooled to room temperature at $5^{\circ}C{\cdot}h^{-1}$ after heated at 180°C for 5 d. Cubic crystals of **IFMC-200** were collected and dried in air (yield 65%, based on H_8L). Elemental analysis: Anal. Calcd for $C_{111}H_{64}O_{72}P_4Zn_{16}$: C 35.84, H 1.73, Zn 28.13, P 3.33; found: C 35.78, H 1.82, Zn 28.05, P 3.26. IR (KBr, cm^{-1}): 3448 (s), 2939 (m), 1626 (s), 1561 (s), 1469 (s), 1425 (s), 1393 (s), 1266 (m), 1138 (m), 1082 (m), 1046 (m), 889 (w), 815 (w), 775 (m), 730 (m), 594 (w), 458 (w).

Sample characterization. The starting material H_8L was synthesized according to modified procedure of the reported literature[40]. All other chemicals were obtained from commercial sources, and were used without further purification. Elemental analyses (C, H and N) were measured on a Perkin-Elmer 2400 CHN elemental analyzer; Zn and P were determined with a Plasma-SPEC(I) ICP atomic emission spectrometer. IR spectrum was performed in the range 4000–400 cm^{-1} using KBr pellets on an Alpha Centaurt FT/IR spectrophotometer. X-ray powder diffraction (XRPD) measurement was recorded radiation ranging from 3 to 60° at room temperature on a Bruker D8 Advance diffractometer with Cu-K_α (λ = 1.5418 Å). Thermogravimetric analysis (TGA) was performed using a Perkin-Elmer TG-7 analyzer heated from room temperature to 900°C under nitrogen at the heating rate of $5^{\circ}C{\cdot}min^{-1}$. Field-emission scanning electron microscopy (FE SEM) images were obtained with a XL30 ESEM FEG microscope equipped with energy dispersive X-ray spectroscopy (EDS).

Determination of acid strength. Titration was used to evaluate the acidic characteristics of the solids. 100 mg of solid samples suspended in 25 mL of NaCl aqueous solution (0.05 $mol{\cdot}L^{-1}$) was stirred for 30 h. Then, acid value was measured by titration with a solution of aqueous ammonia (0.01 $mol{\cdot}L^{-1}$) using phenolphthalein as an indicator.

Catalytic experiments. A 100 mL three-necked glass flask charged with cooled condenser with ~5.0 g of FFAs, a certain amount of anhydrous alcohols and catalyst (**IFMC-200**) in it were vigorously stirred and refluxed (65°C) for the required reaction time. After reaction, the mixture was rotary evaporated at 50°C to separate the excess of alcohols. Then the mixture was left divided into two layers by centrifugation with 4000 rpm. The upper layer was esters of FFAs and the lower layer was **IFMC-200** with small amount of water. The conversion of esters was calculated by measuring the acid value of the products and the yield was detected by gas chromatography (GC). The catalyst was decanted at the bottom of centrifuge, which was easy to be separated, washed by methanol to remove the remaining reactants and water, then dried in air and reused for the next experiment.

Adsorption experiments. The adsorption isotherms of water, ethanol and cyclohexane are measured at 298 K for **IFMC-200**. Before the measurements, the crystalline sample of **IFMC-200** was immersed in CH_2Cl_2 for three days, and then heated at 100°C for 12 h under a vacuum to evacuate the samples.

1. Long, D.-L., Tsunashima, R. & Cronin, L. Polyoxometalates: building blocks for functional nanoscale systems. *Angew. Chem. Int. Ed.* **49**, 1736–1758 (2010).
2. Hayashi, Y. Hetero and lacunary polyoxovanadate chemistry: Synthesis, reactivity and structural aspects. *Coord. Chem. Rev.* **255**, 2270–2280 (2011).
3. Du, D. *et al.* An unprecedented 3D 8-connected pure inorganic framework based on nanosized $\{[Na_{12}PO_{16}H_{24}]\subset[P_4Mo_6O_{31}H_6]_4\}^{15-}$ clusters and zinc cations. *Chem. Commun.* **47**, 2832–2834 (2011).
4. Gao, J. *et al.* Self-assembly of a family of macrocyclic polyoxotungstates with emergent material properties. *Chem. Sci.* **2**, 1502–1508 (2011).
5. Du, D.-Y. *et al.* Polyoxometalate-based crystalline tubular microreactor: redox-active inorganic-organic hybrid materials producing gold nanoparticles and catalytic properties. *Chem. Sci.* **3**, 705–710 (2012).
6. He, P. *et al.* Polyoxometalate-based Supramolecular Gel. *Sci. Rep.* **3**, 1833; DOI:10.1038/srep01833 (2013).
7. Janssens, N. *et al.* Recovery and reuse of heteropolyacid catalyst in liquid reaction medium through reversible encapsulation in $Cu_3(BTC)_2$ metal–organic framework. *Chem. Sci.* **3**, 1847–1850 (2012).
8. Du, D. *et al.* Chiral polyoxometalate-based materials: from design syntheses to functional applications. *Coord. Chem. Rev.* **257**, 702–717 (2013).
9. Liu, J. *et al.* Trimetal lo derivatives of lacunary 9-tungstosilicate heteropolyanions. Part 1 synthesis and characterization. *J. Chem. Soc. Dalton Trans.* 1901–1906 (1992).
10. Ritchie, C. *et al.* Reversible redox reactions in an extended polyoxometalate framework solid. *Angew. Chem. Int. Ed.* **47**, 6881–6884 (2008).
11. Nohra, B. *et al.* Polyoxometalate-based metal organic frameworks (POMOFs): structural trends, energetics, and high electrocatalytic efficiency for hydrogen evolution reaction. *J. Am. Chem. Soc.* **133**, 13363–13374 (2011).
12. Dong, L., Huang, R., Wei, Y. & Chu, W. A remarkable member of the polyoxometalates: the eight-nickel-capped α-Keggin polyoxoazonickelate. *Inorg. Chem.* **48**, 7528–7530 (2009).
13. Dong, L., Li, X., Cao, J., Chu, W. & Huang, R. An α-Keggin polyoxometalate completely constructed from the late transition metal Co^{II} as poly atom. *Dalton Trans.* **42**, 1342–1345 (2013).
14. Marchetti, J. M., Miguel, V. U. & Errazu, A. F. Possible methods for biodiesel production. *Renew. Sust. Energ. Rev.* **11**, 1300–1311 (2007).
15. Melero, J. A., Iglesias, J. & Morales, G. Heterogeneous acid catalysts for biodiesel production: current status and future challenges. *Green Chem.* **11**, 1285–1308 (2009).
16. López, D. E., Goodwin, J. G., Bruce, D. A. & Lotero, E. Transesterification of triacetin with methanol on solid acid and base catalysts. *Appl. Catal. A: Gen.* **295**, 97–105 (2005).
17. Morin, P. *et al.* Transesterification of rapeseed oil with ethanol: I. Catalysis with homogeneous Keggin heteropolyacids. *Appl. Catal. A: Gen.* **330**, 69–76 (2007).
18. Serio, M. D., Tesser, R., Pengmei, L. & Santacesaria, E. Heterogeneous catalysts for biodiesel production. *Energy Fuels* **22**, 207–217 (2008).
19. Xu, Y., Gu, W. & Gin, D. L. Heterogeneous catalysis using a nanostructured solid acid resin based on lyotropic liquid crystals. *J. Am. Chem. Soc.* **126**, 1616–1617 (2004).
20. Tagusagawa, C., Takagaki, A., Hayashi, S. & Domen, K. Efficient utilization of nanospace of layered transition metal oxide $HNbMoO_6$ as a strong, water-tolerant solid acid catalyst. *J. Am. Chem. Soc.* **130**, 7230–7231 (2008).
21. Shultz, A. M., Farha, O. K., Hupp, J. T. & Nguyen, S. T. Synthesis of catalytically active porous organic polymers from metalloporphyrin building blocks. *Chem. Sci.* **2**, 686–689 (2011).
22. Nakajima, K. *et al.* $Nb_2O_5{\cdot}nH_2O$ as a heterogeneous catalyst with water-tolerant Lewis acid sites. *J. Am. Chem. Soc.* **133**, 4224–4227 (2011).
23. Bareyt, S. *et al.* Efficient preparation of functionalized hybrid organic/inorganic Wells−Dawson-type polyoxotungstates. *J. Am. Chem. Soc.* **127**, 6788–6794 (2005).
24. Misono, M. A view on the future of mixed oxide catalysts: The case of heteropolyacids (polyoxometalates) and perovskites. *Catal. Today* **100**, 95–100 (2005).
25. Boglio, C. *et al.* Lanthanide complexes of the monovacant Dawson polyoxotungstate $[\alpha_1\text{-}P_2W_{17}O_{61}]^{10-}$ as selective and recoverable Lewis acid catalysts. *Angew. Chem. Int. Ed.* **45**, 3324–3327 (2006).
26. Gunjakar, J. L., Kim, T. W., Kim, I. Y., Lee, J. M. & Hwang, S. J. Highly Efficient Visible Light-Induced O_2 Generation by Self-Assembled Nanohybrids of Inorganic Nanosheets and Polyoxometalate Nanoclusters. *Sci. Rep.* **3**, 2080; DOI:10.1038/srep02080 (2013).
27. Mizuno, N. & Kamata, K. Catalytic oxidation of hydrocarbons with hydrogen peroxide by vanadium-based polyoxometalates. *Coord. Chem. Rev.* **255**, 2358–2370 (2011).
28. Santacesaria, E., Vicente, G. M., Serio, M. D. & Tesser, R. Main technologies in biodiesel production: State of the art and future challenges. *Catal. Today* **195**, 2–13 (2012).
29. Jiménez-López, A., Jiménez-Morales, I., Santamaría-González, J. & Maireles-Torres, P. Biodiesel production from sunflower oil by tungsten oxide supported on zirconium doped MCM-41 silica. *J. Mol. Catal. A: Chem.* **335**, 205–209 (2011).
30. Shi, W. *et al.* Effects of Brønsted and Lewis acidities on catalytic activity of heteropolyacids in transesterification and esterification reactions. *Chem. Eng. Technol.* **35**, 347–352 (2012).
31. Patel, A. & Narkhede, N. 12-Tungstophosphoric acid anchored to zeolite Hβ: synthesis, characterization, and biodiesel production by esterification of oleic acid with methanol. *Energy Fuels* **26**, 6025–6032 (2012).
32. Shimizua, K. & Satsuma, A. Toward a rational control of solid acid catalysis for green synthesis and biomass conversion. *Energy Environ. Sci.* **4**, 3140–3153 (2011).
33. Moll, H. E. *et al.* Lanthanide polyoxocationic complexes: experimental and theoretical stability studies and Lewis acid catalysis. *Chem. Eur. J.* **17**, 14129–14138 (2011).
34. Suzuki, K. *et al.* Strategic design and refinement of Lewis acid−base catalysis by rare-earth-metal-containing polyoxometalates. *Inorg. Chem.* **51**, 6953–6961 (2012).
35. Xu, L. *et al.* Simultaneous esterification and transesterification of soybean oil with methanol catalyzed by mesoporous Ta_2O_5/SiO_2–$[H_3PW_{12}O_{40}/R]$ (R = Me or Ph) hybrid catalysts. *Green Chem.* **11**, 314–317 (2009).
36. Brahmkhatri, V. & Patel, A. Esterification of lauric acid with butanol-1 over $H_3PW_{12}O_{40}$ supported on MCM-41. *Fuel* **102**, 72–77 (2012).
37. Sun, C. *et al.* Highly stable crystalline catalysts based on a microporous metal-organic framework and polyoxometalates. *J. Am. Chem. Soc.* **131**, 1883–1888 (2009).

38. Du, D. *et al.* Redox-active polyoxometalate-based crystalline material-immobilized noble metal nanoparticles: spontaneous reduction and synergistic catalytic activity. *J. Mater. Chem.* **22**, 21040–21044 (2012).
39. Yang, X.-L. *et al.* Porous metalloporphyrinic frameworks constructed from metal 5,10,15,20-tetrakis(3,5-biscarboxylphenyl)porphyrin for highly efficient and selective catalytic oxidation of alkylbenzenes. *J. Am. Chem. Soc.* **134**, 10638–10645 (2012).
40. Lan, Y., Jiang, H., Li, S. & Xu, Q. Solvent-induced controllable synthesis, single-crystal to single-crystal transformation and encapsulation of Alq3 for modulated luminescence in (4,8)-connected metal−organic frameworks. *Inorg. Chem.* **51**, 7484–7491 (2012).
41. Ballirano, P. & Maras, A. Refinement of the crystal structure of arsenolite, As_2O_3. *Z. Kristallogr. NCS* **217**, 177–178 (2002).
42. Keggin, J. F. Structure of the molecule of 12-phosphotungstic acid. *Nature* **131**, 908–909 (1933).
43. López, X., Carbó, J. J., Bo, C. & Poblet, J. M. Structure, properties and reactivity of polyoxometalates: a theoretical perspective. *Chem. Soc. Rev.* **41**, 7537–7571 (2012).
44. Spek, A. L. Single-crystal structure validation with the program *PLATON*. *J. Appl. Cryst.* **36**, 7–13 (2003).
45. O'Keeffe, M., Peskov, M. A., Ramsden, S. J. & Yaghi, O. M. The Reticular chemistry structure resource (RCSR) database of, and symbols for, crystal nets. *Acc. Chem. Res.* **12**, 1782–1789 (2008).
46. Delgado-Friedrichs, O. & O'Keeffe, M. Identification of and symmetry computation for crystal nets. *Acta Crystallogr.* **A59**, 351–360 (2003).
47. O'Keeffe, M. & Yaghi, O. M. Deconstructing the crystal structures of metal-organic frameworks and related materials into their underlying nets. *Chem. Rev.* **112**, 675–702 (2012).
48. Perry IV, J. J., Kravtsov, V. Ch., McManus, G. J. & Zaworotko, M. J. Bottom up synthesis that does not start at the bottom: quadruple covalent cross-linking of nanoscale faceted polyhedra. *J. Am. Chem. Soc.* **129**, 10076–10077 (2007).
49. Yuan, D., Zhao, D., Sun, D. & Zhou, H.-C. An isoreticular series of metal–organic frameworks with dendritic hexacarboxylate ligands and exceptionally high gas-uptake capacity. *Angew. Chem. Int. Ed.* **49**, 5357–5361 (2010).
50. Zheng, S.-T. *et al.* Multicomponent self-assembly of a nested $Co_{24}@Co_{48}$ metal–organic polyhedral framework. *Angew. Chem. Int. Ed.* **50**, 8034–8037 (2011).
51. Ramsden, S. J., Robins, V. & Hyde, S. T. Three-dimensional Euclidean nets from twodimensional hyperbolic tilings: kaleidoscopic examples. *Acta Cryst.* **A65**, 81–108 (2009).
52. Morris, W. *et al.* Synthesis, structure, and metalation of two new highly porous zirconium metal-organic frameworks. *Inorg. Chem.* **51**, 6443–6445 (2012).
53. Wang, X. *et al.* Self-assembly of nanometer-scale $[Cu_{24}I_{10}L_{12}]^{14+}$ cages and ball-shaped Keggin clusters into a (4,12)-connected 3D framework with photoluminescent and electrochemical properties. *Angew. Chem. Int. Ed.* **45**, 7411–7414 (2006).
54. Samms, S. R., Wasmus, S. & Savinell, R. F. Thermal stability of nafion® in simulated fuel cell environments. *J. Electrochem. Soc.* **143**, 1498–1504 (1996).
55. Sharma, Y. C., Singh, B. & Korstad, J. Latest developments on application of heterogenous basic catalysts for an efficient and eco friendly synthesis of biodiesel: A review. *Fuel* **90**, 1309–1324 (2011).
56. Liu, F. *et al.* Transesterification catalyzed by ionic liquids on superhydrophobic mesoporous polymers: heterogeneous catalysts that are faster than homogeneous catalysts. *J. Am. Chem. Soc.* **134**, 16948–16950 (2012).
57. Zhang, D., Barri, S. A. I. & Chadwick, D. Dehydration of 1,2-propanediol to propionaldehyde over zeolite catalysts. *Appl. Catal. A: Gen.* **400**, 148–155 (2011).
58. Kokubo, M., Ogawa, C. & Kobayashi, S. Lewis acid catalysis in water with a hydrophilic substrate: scandium-catalyzed hydroxymethylation with aqueous formaldehyde in water. *Angew. Chem. Int. Ed.* **47**, 6909–6911 (2008).
59. Liu, Y., Lotero, E. & Goodwin, J. G. Jr. Effect of carbon chain length on esterification of carboxylic acids with methanol using acid catalysis. *J. Catal.* **243**, 221–228 (2006).
60. Inumaru, K., Ishihara, T., Kamiya, Y., Okuhara, T. & Yamanaka, S. Water-tolerant, highly active solid acid catalysts composed of the Keggin-type polyoxometalate $H_3PW_{12}O_{40}$ immobilized in hydrophobic nanospaces of organomodified mesoporous silica. *Angew. Chem. Int. Ed.* **46**, 7625–7628 (2007).

Acknowledgments

This work was financially supported by Pre-973 Program (2010CB635114), the National Natural Science Foundation of China (No. 21001020) and Graduate Innovation Fund of Jilin University (No. 20121048).

Author contributions

D.Y.D. and J.S.Q. carried out the experiments and wrote the paper. Z.S. and X.H.W. performed the biodiesel preparation experiment. L.K.Y. calculated the frontier molecular orbitals. M.O. performed the topology analysis. Z.M.S., S.L.L., X.L.W. and Y.Q.L. supervised the research and revised the manuscript. All authors reviewed the manuscript.

Additional information

Supplementary information accompanies this paper at http://www.nature.com/scientificreports

Competing financial interests: The authors declare no competing financial interests.

How to cite this article: Du, D. *et al.* An unprecedented (3,4,24)-connected heteropolyoxozincate organic framework as heterogeneous crystalline Lewis acid catalyst for biodiesel production. *Sci. Rep.* **3**, 2616; DOI:10.1038/srep02616 (2013).